Electronic Supplementary Material (ESI) for Nanoscale.
This journal is © The Royal Society of Chemistry 2023

SUPPORTING INFORMATION to

ZIF-8 Thin films by a Vapor-phase Process: Limits to growth

Virginie Perrot[a,b], Arthur Roussey[c], Anass Benayad[c], Marc Veillerot[a], Denis Mariolle[a], Albert Solé-Daura[d,†], Caroline Mellot-Draznieks[d], Florence Ricoul[a], Jérôme Canivet[b], Elsje A. Quadrelli*[b], Vincent Jousseaume*[a]

[a] Univ. Grenoble Alpes, CEA, LETI, F-38000 Grenoble, France

[b] University Of Lyon, Institut De Chimie De Lyon, IRCELYON UMR 5256–CNRS–Université Lyon 1, Institut de recherche sur la catalyse et l'environnement, Villeurbanne, France

[c] Univ. Grenoble Alpes, CEA, LITEN, F-38000 Grenoble, France

[d] Laboratoire de Chimie des Processus Biologiques, UMR CNRS 8229, Collège de France, Sorbonne Université, PSL Research University, 11 Place Marcelin Berthelot, 75231 Paris Cedex 05, France.

I. Determination of the film thickness by spectroscopic ellipsometry

In this work, the samples were composed of a stack of three materials: the silicon substrate, the residual ZnO and the formed ZIF-8 layer. For the silicon substrate, the optical constants were fixed for all measurements and its thickness was considered infinite. The optical constants of ZnO were determined and fixed by prior measurements of a ZnO/Si sample after ALD deposition. They were modelled by a set of oscillators as described in literature.[1] The value of the refractive index at 632 nm is 1.94 in agreement with other works.[2] To evaluate the thickness and the refractive index of the ZIF-8 layer, two common models were confronted. The first one is the Cauchy model involving three parameters (An, Bn, and Cn). In that case, the refractive index depends on these parameters and on the wavelength λ (nm):

$$n(\lambda) = A_n + \frac{B_n}{\lambda^2} + \frac{C_n}{\lambda^4} \qquad \text{(Equation S1)}$$

To simulate the absorption of light, an Urbach absorption "tail" was added to model the evolution of the extinction coefficient for wavelengths below the value of the Band Edge which was fixed at 400 nm (equation S2):

$$k(\lambda) = k_{amplitude} \exp\left(Exponent\left(\frac{1{,}24}{\lambda} - \frac{1{,}24}{\gamma}\right)\right) \qquad \text{(Equation S2)}$$

The Cauchy model has already been used in the literature for estimating the thickness and refractive index of ZIF-8 layer by ellipsometry.[3,4]

The second model, the Tauc-Lorentz oscillator is a parameterization of the dielectric function usually used to describe the optical properties of amorphous semiconductor materials and polymers. The dielectric function is calculated from the model established by Tauc *et al.*[5] and the

standard Lorentz model.[6] It combines in the expression of the imaginary part of the total dielectric function $\varepsilon i,_{TL}$ the product of the imaginary part of the Tauc dielectric function $\varepsilon i,_{T}$ by the Lorentz one $\varepsilon i,_{L}$ (Equation S3):

$$\varepsilon_{TL}(E) = \varepsilon_{r,TL} + i(\varepsilon_{i,T}\varepsilon_{i,L})$$ (Equation S3)

with

$$\varepsilon_{i,T}(E > E_g) = A_T\left(\frac{E - E_g}{E}\right)^2$$ (Equation S4)

where A_T is the Tauc coefficient related to the amplitude of the dielectric function, E is the energy of the photons, E_g is the energy of the optical gap and a simple Lorentz oscillator described by the following mathematical form:

$$\varepsilon_{i,L}(E) = \frac{A_L.E_0.B_r.E}{\left(E^2 - E_0^2\right) + B_r^2E^2}$$ (Equation S5)

Where A_L is related to the amplitude of the Lorentz oscillator, B_r is the broadening term of the extinction peak and E_0 is the energy position of the extinction peak. The real part ε(r,TL) is given by the Kramers-Kronig integral.[7]

For each model, the addition of an additional roughness layer located on the top of the ZIF-8 layer was evaluated. This layer combines the optical index of the ZIF layer and the index of the air by an effective medium approximation (EMA).[8,9] Figure S1 shows the stacks considered for the modeling.

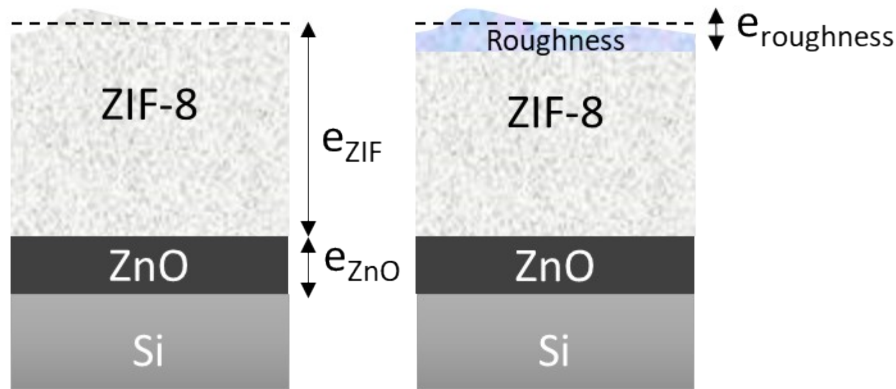

Figure S1 : Stacks considered for modeling. The ZIF-8 layer is modeled by the Cauchy or Tauc-Lorentz model with or without a roughness layer.

For all regressions, the Si substrate parameters were fixed as well as the ZnO optical indices. The parameters that vary were the thicknesses of ZnO (eZnO) and the ZIF layer (eZIF) as well as some parameters of the ZIF index. In the case where a "roughness layer" was added, its thickness ($e_{roughness}$) is an additional unknown parameter.

Table S1. Example of results obtained by fitting the ellispometry data with different models on a **ZIF-8@10_exposures** sample after its synthesis (and without any activation).

Model	ZIF-8 thickness (nm)	ZnO thickness (nm)	Refractive index (n) at 632 nm	Mean Square Error	Roughness (nm)
Cauchy	79.0	48.3	1.47	38	/
Cauchy with roughness	78.9	46.5	1.50	35	20.4
Tauc-Lorentz Oscillator	77.7	48.4	1.48	37	/
Tauc-Lorentz Oscillator with roughness	77.2	47.7	1.50	36	19.8
Average	78.2	47.7	1.49		20
Standard deviation	0.89	0.87	0.02		0.42

Table S1 shows the results of the different fits that were performed over the wavelength range [250-1700 nm] for a measurement at the centre of a ZIF-8@10_exposures sample after its synthesis and without any activation.

On the one hand, the average value obtained for the thickness of the ZIF-8 layer is 78.2 nm with a standard deviation of 0.9 nm. The ZnO layer has a thickness of about 47.7 nm with a standard deviation of 0.9 nm. As all these models are converging towards close thickness values, anyone of these models can be used and it is then possible to compare the thickness of the layers between them.

On the other hand, the optical index n of the ZIF-8 layer varies significantly from 1.47 to 1.50 depending of the model used. Modelization relying on ellipsometry often allows to reach an accuracy lower than 0.01 on the refractive index. This is not the case for our ZIF-8 thin films. The addition of a roughness layer in the fit does not significantly decrease the mean square error (MSE) value and add an additional parameter, which increases the uncertainty of the fit.

The starting ZnO layer being about 50 nm (± 1 nm), there is a significant expansion between the thickness of the ZIF-8 layer formed and the ZnO layer consumed. Indeed, between 2 and 4 nm of ZnO were consumed to form more than 70 nm of ZIF-8. The theoretical value of the expansion is 17 in the case of ZIF-8 formed from a dense ZnO. The uncertainty in the thicknesses does not allow us to calculate this expansion factor accurately. In this example, we can estimate a factor higher than 19, which is more than the theoretical value but confirms the production of a less dense layer.

The MSE (Mean square value) is quite high as an ideal fit leads to a MSE close to 1. This can be explained by the roughness of the layer which can lead to a slight depolarization of the light[7] and

disturbs the quality of the collected signal. The different models leading to similar MSE, the Cauchy model without roughness was chosen because it is the model with the fewest regression parameters and it gives similar results to the Tauc-Lorentz model. Figure S2 shows an example of experimental data of ψ and Δ and the modeling with the Cauchy model for the ZIF-8@10_exposures sample. A fairly good agreement is obtained between the model and the experimental data.

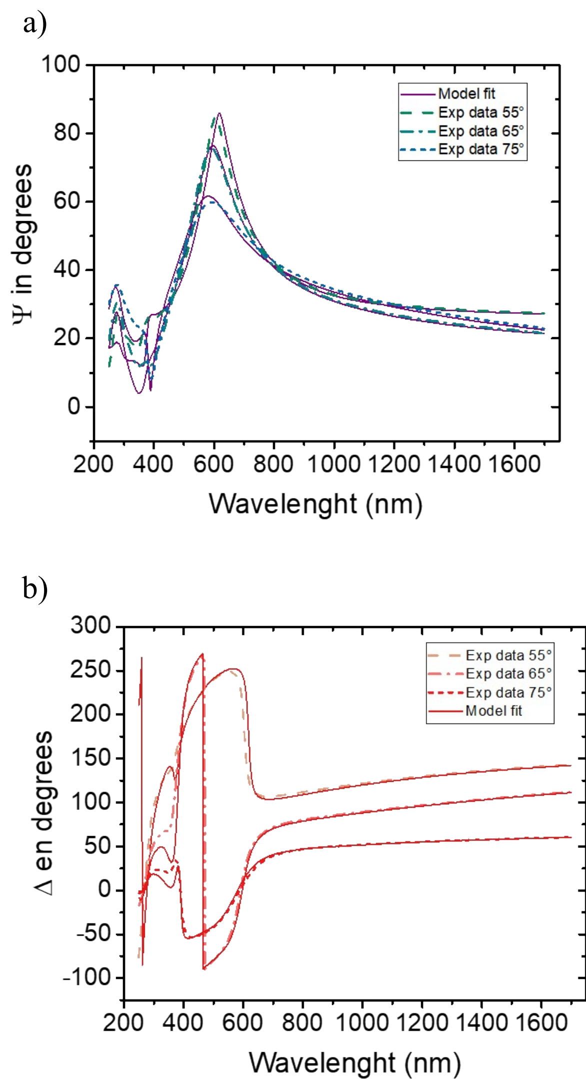

Figure S2 : Experimental and modeling data of the Cauchy model of (a) ψ and (b) Δ measured by spectroscopic ellipsometry at 3 different angles (55, 65, and 75°) for a ZIF@10_exposures sample.

II. FTIR

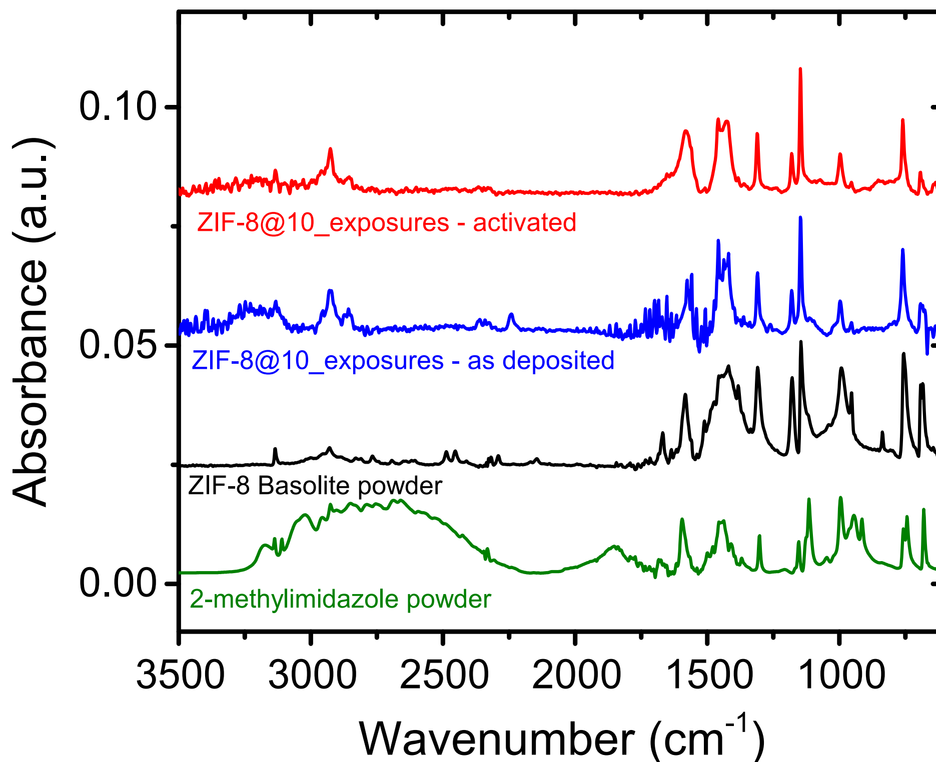

Figure S3. FT-IR spectrum of one typical sample after 10 exposures (ZIF-8@10_exposures), as deposited (in blue) and after activation (in red), 2-methylimidazole (MeIm-H) powder (in green) and ZIF-8 commercial Basolite powder (in black) for reference.

Expected infrared vibrations of ZIF-8 are obtained in the FTIR spectra (Figure S3): the aromatic ν(CH) at 3134 cm^{-1} and ν(C=N) at 1580 cm^{-1} and in-plane and out-of-plane bending modes of the ring, respectively between 1450-900 cm^{-1} and below 800 cm^{-1}. Note that a signal at 2925 cm^{-1}, typically observed for ν(CH_2) is observed on the as-deposited sample and is attributed to organic contamination as it disappears upon activation. Another signal at 2240 cm^{-1}, unassigned, is also likely due to contamination as it is not visible in the activated sample. Further comparison with 2-

methylimidazole, which exhibits a strong and broad band centered around 2750 cm^{-1} and a band at 1842 cm^{-1} assigned to the NH–N hydrogen bonds, absent from ZIF-8, confirmed that the 2-methylimidazole linkers were fully deprotonated during the formation of the ZIF structure.

III. Pore size distribution

From the isotherms obtained by Ellipsometry-Porosimetry, it is possible to estimate the pore size based on the Kelvin's equation.[10] The model is based on the capillary condensation of the solvent in spherical pores. The following figure S4 shows the pore size distribution deduced using this model. A monodisperse pore size distribution is obtained with a mean pore radius close to 0.6 nm. This is in good agreement with the theoretical value expected for ZIF-8 (0.58 nm).

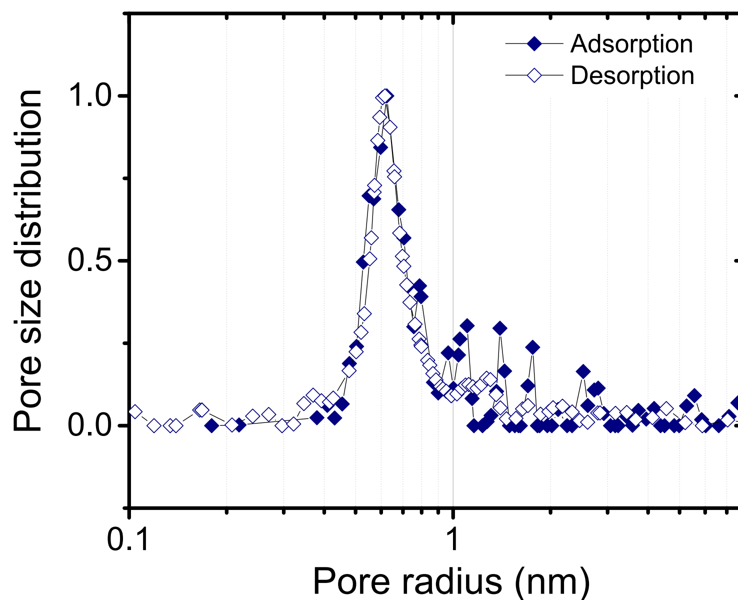

Figure S4. Example of pore size distribution of ZIF-8@5 exposures determined from the EP isotherms

It is important to underline that the Kelvin's model is at the limit of its validity. Indeed, for pore radius below 1 nm (micropores), capillary condensation monolayer by monolayer is probably not the mechanism governing the filling of the pores. This method allows to obtain an order of magnitude for the mean pore size but is difficult to use in order to compare samples that are very close from each others.

IV. Water contact Angle

Water contact angle (WCA) experiments was studied as a function of the water vapour pressure used during the growth (samples corresponding to Figure 3a). Figure S5 shows the variations of WCA for as-deposited and activated samples. No clear trend is detected. As-grown ZIF-8 layers present WCA close to 110° while activated samples present WCA close to 90°-95°.

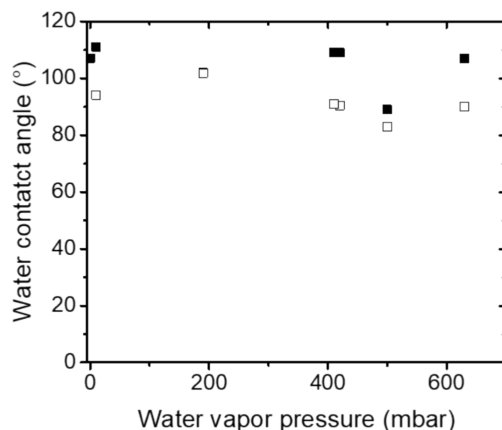

Figure S5. Variation of the water contact angle for ZIF-8 samples grown using different water vapor pressures. Black squares are for as-grown sample and open square were measured after activation.

V. TOF-SIMS profiles

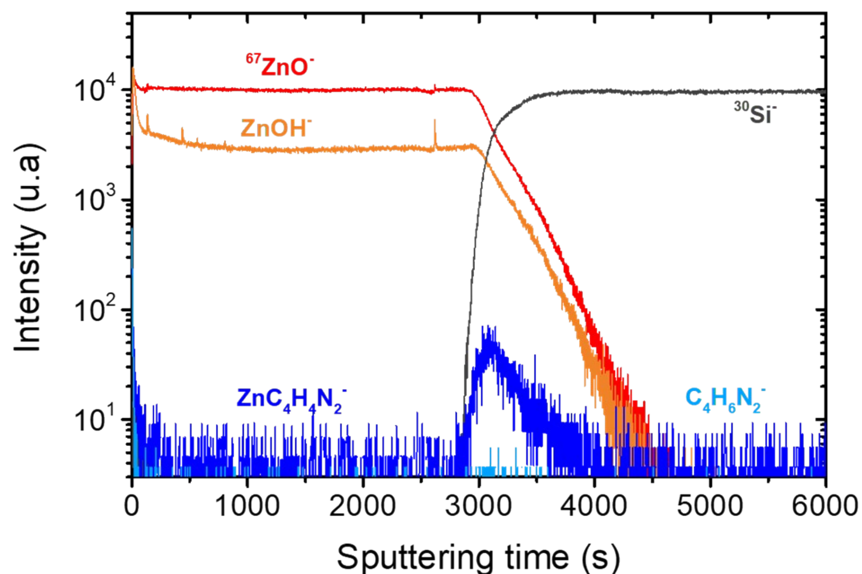

Figure S6. TOF-SIMS Profile of the stack ZIF-8@3_exposures / ZnO / Si

VI- XPS

X-ray Photoelectron Spectroscopy (XPS) measurements were performed using a VersaProbe II (ULVAC-PHI) spectrometer equipped with a monochromatized micro-focused (beam size 100 μm^2) X-ray source (Al Kα 1486.6 eV). The takeoff angle was 45° relative to the substrate surface. The energetic resolution was 0.5 eV. The measurements were carried out by first monitoring a survey spectrum of wide binding energy region (0-1092 eV) with a pass energy of 117 eV. High resolution spectra were recorded using a pass energy of 23 eV to record the Zn 2p, Zn LMM, O 1s, N 1s and C 1s core level peaks regions for all samples. The data analysis was performed with Multipak software. All spectra were calibrated relatively to the contribution (C-C, C-H) of the C 1s at 284.8 eV. The peaks were fitted by a pseudo-voigt function (sum of Gaussian and Lorentzien

curves with of ratio fixed at 80/20 %). In the case of in depth XPS analyses, the samples were transferred in the spectrometer using airtight transfer vessel to avoid air contamination. XPS depth profiling were performed using focused Argon ions beam with acceleration energy of 1 KeV and one minute sputtering step.

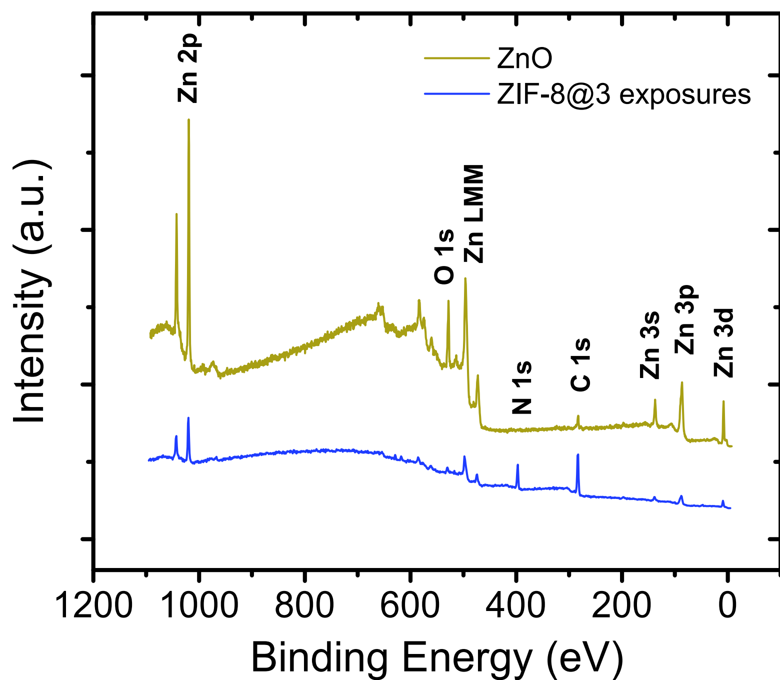

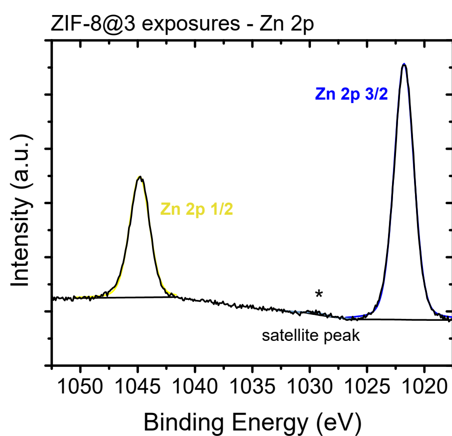

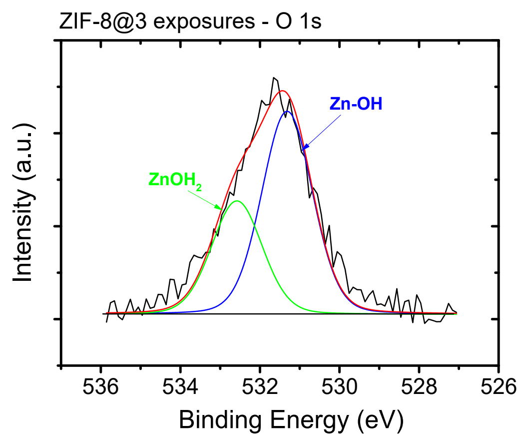

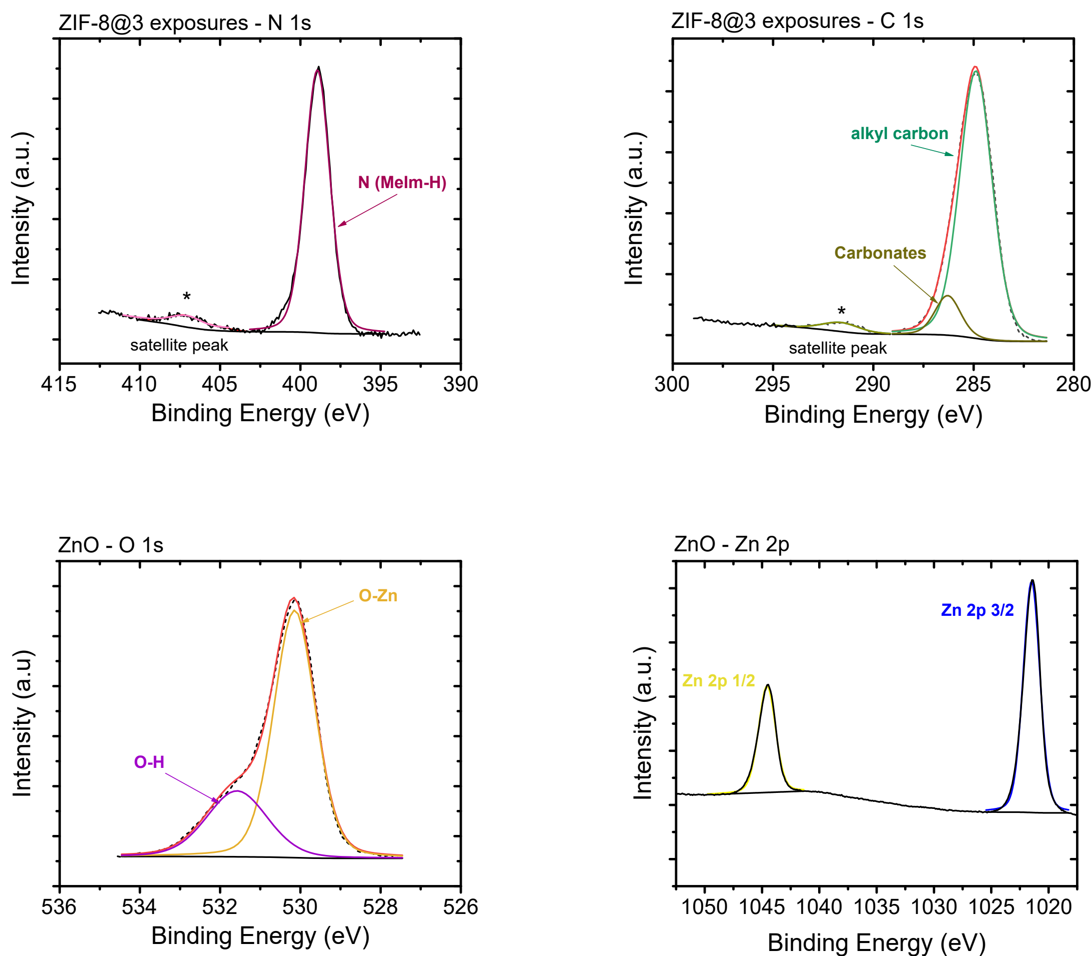

Figure S7. XPS Surveys and high resolution Zn 2p, O 1s, N 1s, C 1s core level spectra of **ZIF-8@3_exposures** and O 1s and Zn 2p spectra of ZnO

VI.1. ZnO

For ZnO, the stoichiometry obtained by XPS is close to the expected one (1:1 for Zn:O). The presence of carbon on the surface of the ZnO can be partly due to an organic contamination and to carbon residues from the ALD deposition process (the zinc precursor being the diethylzinc). In the case of the ZIF-8 thin film, the C/N atomic ratio is ~2.8 (compare to 2.3 for the Basolite powder). This value, higher than the theoretical one (C/N=2), can also be due to a surface organic

contamination or to the presence of organic molecules adsorbed in the porosity. The N/Zn atomic ratio is close to 2.9 for both the **ZIF-8@3_exposures** and the commercial Basolite whereas the theoretical ratio is 4. The surface would thus be enriched in zinc terminations not linked to imidazole groups as already observed and described by Sharma *et al.*[11]

The C 1s region of the ZnO can be decomposed into several components: the main one at 284.8 eV corresponds to the aliphatic C-C and C-H carbons and the other two are attributed to CO and COOH (286.1 and 289 eV respectively) (Figure S5).

VI.2. ZIF-8

Based on the measurement conditions and the density of ZIF-8, the depth of the material probed by the photoelectrons is about 6-10 nm for the **ZIF-8@3_exposures**, which is less than the thickness of the ZIF-8 layer estimated by ellipsometry (20 nm). The ZnO layer underneath the ZIF-8 layer is therefore not expected to be analyzed. Since the main peak in the N 1s region of ZIF-8 is symmetric, it was fitted with only one contribution at 398.9 eV and attributed to the overlap of N-Zn and N-C bonds of the ligand (Figure S7).[11] A small additional contribution can eventually be detected at 400.2 eV (indicated by an arrow in Figure S7) and is probably due to the nitrogen bonds of the imidazolate groups.[12] The C 1s spectrum can be decomposed into two contributions: a main one at 284.9 eV attributed to the alkyl carbons (C-C and C-H bonds) of the 2-methylimidazolate in the ZIF structure and a smaller one at higher energy that can be attributed to contamination from carbonates.[11,13] The positions of the two Zn $2p_{3/2}$ and Zn $2p_{1/2}$ peaks are 1021.5-1044.6 eV and 1021.8-1044.8 eV for ZnO and ZIF-8, respectively. The distance between the Zn $2p_{3/2}$ and Zn $2p_{1/2}$ peaks (derived from the spin-orbit splitting of 23 eV) confirms the +2

valence state in both samples (Figure S7).[12,14] The appearance of satellite peaks for the core level peaks of Zn $2p_{3/2}$, N 1s, and C 1s after conversion in ZIF-8 confirms the presence of the deprotonated ligand. Indeed, these satellite peaks are attributed to delocalized π-conjugation ($\pi \rightarrow \pi^*$) in the ZIF-8 lattice.[15-16]

VII – Simulation

Computational modelling of defective models of ZIF-8: The defective models of ZIF-8 (n missing linkers) were derived from the defect-free supercell of ZIF-8 using a Monte Carlo approach in order to ensure the random distribution of defects, whereby n+1 negatively charged atoms were docked into an artificially positively n+ charged ZIF-8 framework. The n imidazolate linkers that were the closest to the n docked anions were designated as missing linkers, and replaced each by a hydroxo and an aqua ligand for completing the coordination of the two involved Zn centers.

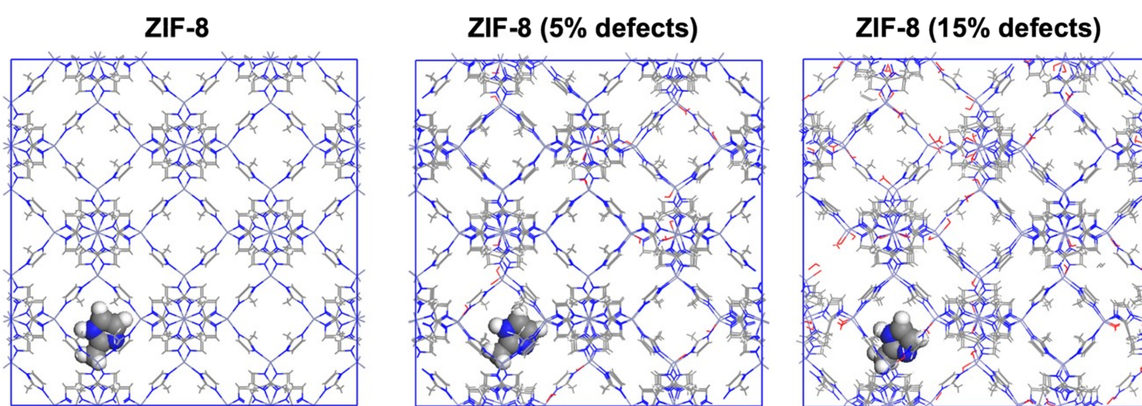

Figure S8. Snapshots of the cubic, 3D-periodic simulation boxes used to run and analyze the dynamic behavior of a MeIm-H molecule (represented in spheres) inside a pristine ZIF-8 (left),

and defective ZIF-8 containing 5% (middle) and 15% (right) of defects. Box dimensions: 33.763^3 $Å^3$ (2 × 2 × 2 supercell). Defects (coordinated H_2O molecules and –OH groups) are colored in red.

VIII – AFM

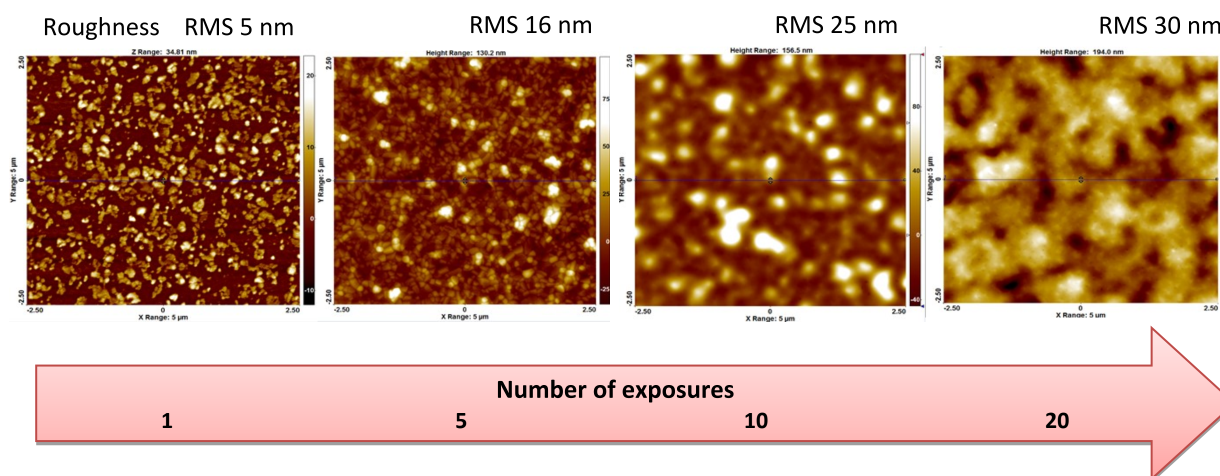

Figure S9. AFM images of ZIF-8 samples for different exposures.

REFERENCES

(1) P. L. Washington, H. C. Ong, J. Y. Dai, R. P. H. Chang, *Appl. Phys. Lett.* 1998, **72**, 3261-3263.

(2) Y. C. Liu, J. H. Hsieh, S. K. Tung, *Thin Solid Films* 2006, **510**, 32-38.

(3) A. J. Cruz, I. Stassen, M. Krishtab, K. Marcoen, T. Stassin, S. Rodríguez-Hermida, J. Teyssandier, S. Pletincx, R. Verbeke, V. Rubio-Giménez, S. Tatay, C. Martí-Gastaldo, J. Meersschaut, P. M. Vereecken, S. De Feyter, T. Hauffman, R. Ameloot, *Chem. Mater.* 2019, **31**, 9462-9471.

(4) A. Demessence, C. Boissière, D. Grosso, P. Horcajada, C. Serre, G. Férey, G. J. A. A. Soler-Illia, C. Sanchez, *J. Mater. Chem.* 2010, **20**, 7676.

(5) J. Tauc, R. Grigorovici, A. Vancu, *Phys. Status Solidi B* 1966, **15**, 627-637.

(6) R. M. A. Azzam, N. M. Bashara, Ellipsometry and Polarized Light; North-Holland Pub. Co. ; sole distributors for the U.S.A. and Canada, Elsevier North-Holland: Amsterdam ; New York, 1977.

(7) H. Fujiwara, Spectroscopic Ellipsometry: Principles and Applications; John Wiley & Sons: Chichester, England ; Hoboken, NJ, 2007.

(8) D. Rönnow, S. K. Anderson, G. A. Niklasson, *Opt. Mater.* 1995, **4**, 815-821.

(9) D. E. Aspnes, J. B.Theeten, F. Hottier, *Phys. Rev. B* 1979, **20**, 3292-3302.

(10) M.R. Bakalnov, K. P. Mogilnikov, V. G. Polovinkin, F. N. Dultsev, *J. Vac. Sci. Technol. B* 2000, **18**, 1385.

(11) S. K. Sharma, P. Utpalla, J. Bahadur, U. K. Goutam, P. K. Pujari, *Microporous and Mesoporous Materials* 2020, **307**, 110519.

(12) C. D. Wanger, W. M. Riggs, L. E. Davis, J. F. Moulder and G. E.Muilenberg, Handbook of X-Ray Photoelectron Spectroscopy Perkin-Elmer Corp., Physical Electronics Division, Eden Prairie, Minnesota, USA, 1979.

(13) F. Tian, A. M. Cerro, A. M. Mosier, H. K. Wayment-Steele, R. S. Shine, A. Park, E. R. Webster, L. E. Johnson, M. S. Johal, L. Benz, *J. Phys. Chem. C* 2014, **118**, 14449-14456.

(14) J. Liu, J. He, L. Wang, R. Li, P. Chen, X. Rao, L. Deng, L. Rong, J. Lei, *Sci. Rep.* 2016, **6**, 23667.

(15) S. Gadipelli, W. Travis, W. Zhou, Z. A. Guo, *Energy Environ. Sci.* 2014, **7**, 2232-2238.

(16) J. E. Morales-Ugarte, C. C. Santini, R. Bouchet, A. Benayad, *J. Phys. Chem. B* 2020, **124**, 7625-7635.